Unveiling a critical thickness in photocatalytic TiO 2 thin films grown by plasma-enhanced chemical vapor deposition using real time in situ spectroscopic ellipsometry

W Ravisy, M Richard-Plouet, B Dey, S Bulou, P Choquet, A Granier, A Goullet

Unveiling a critical thickness in photocatalytic TiO_2 thin films grown by Plasma-Enhanced Chemical Vapor Deposition using dynamic *in situ* spectroscopic ellipsometry

W. Ravisy[1], M. Richard-Plouet[1], B. Dey[2], S. Bulou[2], P. Choquet[2], A. Granier[1], A. Goullet[1]

[1]Université de Nantes, CNRS, Institut des Matériaux Jean Rouxel, IMN, F-44000 Nantes, France

[2]Materials Research and Technology Department, Luxembourg Institute of Science and Technology, 5 Avenue des Hauts-Fourneaux, 4362 Esch-sur-Alzette, Luxembourg

Abstract

TiO_2 thin films of various thicknesses have been deposited on silicon at low-temperature by PECVD operating in continuous mode (T<130°C) and pulsed mode (T<80°C) using oxygen / Titanium Isopropoxide low-pressure inductively coupled plasma. The study of the crystallinity and microstructure of the films by AFM, SEM and XRD allowed showing that the roughness and amount of anatase are closely related to the film thickness. The coalescence of large polycrystalline columns emerging from an assembly of thin columns was found to happen at a critical thickness, at about 150 nm in the continuous mode and 250 nm in the pulsed mode. Dynamic *in situ* spectroscopic ellipsometry study allowed to monitor the growth and to determine this critical thickness for both plasma modes. The change of morphology type to large columnar structure is associated with an important increase in the photocatalytic activity. The determination of this coalescence thickness by ellipsometry may provide an interesting method to evaluate the impact of process parameters on TiO_2 thin films characteristics.

1. Introduction

Titanium dioxide (TiO_2) has been extensively studied over the past decades due to its photoactive properties under UV exposure.(1,2) It is commonly accepted for photocatalytic applications that anatase is the most interesting polymorph.(3) If several techniques allow depositing TiO_2 thin films (sputtering, sol-gel…), a temperature above 200°C is almost always mandatory to achieve anatase crystallization, whether is it during the deposition process or as a post-treatment.(4–8) Thus, temperature sensitive substrates, namely stiff and flexible polymers, are often discarded in favor of heat resistant rigid substrates such as glass or silicon. Yet, polymers have many beneficial properties, such as low weight, low cost or flexibility.(9) In particular, functional transparent organic flexible substrates are expected to take a larger place in the fabrication of new products. The deposition of photocatalytic material on flexible polymer substrates could lead to easy-to-handle and easy-to-shape devices for antibacterial, antifouling or wastewater treatment applications,(10) and would allow dynamic deposition with roll-to-roll processing for example.

Except works involving sol-gel process(11–13), few studies have been dedicated to the direct deposition of crystallized TiO_2 thin films at low temperature. Nearly all of them rely on plasma assisted deposition techniques, such as High Power Impulse Magnetron Sputtering (HiPIMS)(14–16), Plasma-Enhanced Atomic Layer Deposition (PE-ALD)(17,18) or Plasma-Enhanced Chemical Vapor Deposition (PECVD).(19–22) HiPIMS has been optimized to allow depositing a mixture of anatase, rutile and brookite on Polyethylene Terephthalate (PET) and Polycarbonate (PC) without damaging the substrates(15). PE-ALD(23) and self-limiting Pulsed PECVD processes(24), relying on cycles of alternating precursor injection and plasma discharge, have also proven to lead to deposit anatase at low temperature (namely 110°C and 120°C).

Previous works from our group have also shown that low-pressure Plasma Enhanced Chemical Vapor Deposition (PECVD) was particularly suitable to deposit anatase crystallized TiO_2 thin films below 150°C.(25) Moreover, pulsing the plasma discharge (frequency of 1 kHz and duty cycle of 50%) was found to decrease the temperature down to 80°C while maintaining anatase formation at the surface of the film.(26) With this technique, photocatalytic TiO_2 has been deposited on PET/ITO (PET film with a 50 nm thin film of Tin doped Indium Oxide) and Polystyrene (PS) substrates. Pulsed discharge PECVD (Pulsed-PECVD) thus appears as a very promising process for producing flexible, easy to manipulate photocatalytic films. However, the growth mechanism of anatase in these low-temperature low-pressure PECVD and Pulsed-PECVD processes remains poorly known.

As-deposited low-temperature PECVD TiO_2 thin films are often defined as amorphous by X-Ray diffraction or Raman scattering analysis.(20,19,27,28) In oxygen rich plasmas, their morphology is characterized by thin parallel columns of roughly 10 nm in diameter.(29,30) Borras et al defined a critical thickness at which the growth switches from an initial homogeneous regime, governed by the diffusion of species, to the prevalence of a shadowing phenomenon resulting in the narrow columnar morphology.(31,32) In the literature, crystallization of the as-deposited thin films is only reported when process temperature exceeds 200°C. (33–35) All of the crystallized TiO_2 thin films deposited by PECVD exhibit a columnar growth, with wide polycrystalline columns, whose diameter is of the order of several tens of nanometers. The Kolmogorov model (KM), if originally describing crystal growth from an homogeneous environment, was found suitable to describe polycrystalline TiO_2 columnar growth by PECVD at 250°C.(25,32,33) The KM decomposes growth in four steps: *1) Nucleation of crystal domains 2) Coalescence 3) Columns formation* and *4) Columns development*. Specifically, the nucleation step of the crystal growth was determined to be critical for microstructural domains formation.(33) The columns development step was reported as a competitive growth, with columns growing both vertically and horizontally, inducing a V-shape and possible hindrance.(34,36,37)

To this day, no work has thoroughly addressed the growth mechanism of TiO_2 thin films deposited in Pulsed-PECVD. A gradual crystallization of anatase along the growth direction was evidenced by Selective Area Electron Diffraction (SAED) in 300 nm thick films: anatase crystallization was shown to be gradually improved toward the surface.(26) Similar observation was made in classic PECVD by Lee et al, where long deposition times allowed an amorphous thin film to partially crystallize in the anatase phase.(19) This suggests that thickness is a key parameter for the crystallization of TiO_2 thin films in PECVD, and thus may have strong impact on photocatalytic properties.

This work aims to relate the characteristics and properties of the anatase TiO_2 films deposited in low-temperature PECVD and Pulsed-PECVD to the growth mechanism. By varying the deposition time, thin films of different thicknesses have been deposited in the two modes: continuous and pulsed plasma. The dependence of the as-deposited films morphology, crystalline structure and photocatalytic properties on thickness and plasma discharge mode are discussed. A major interest of this work is that dynamic real time in situ spectroscopic ellipsometry is used to monitor film growth and quality with regard to the application. Indeed, this approach allows determining in real-time film thickness and roughness evolutions, which are directly related to the photocatalytic activity.(38) Fundamentally, it can also provide original insights on the growth mechanism involved.

2. Materials and Methods

TiO_2 thin films have been deposited on (100)-oriented Si in a radiofrequency (13.56 MHz) inductively coupled plasma enhanced chemical vapor deposition reactor, represented in Figure 1 and described in details elsewhere,(39) working at low pressure (~0.4 Pa). A power of 400 W was injected into the plasma source and all the films were deposited at floating potential.

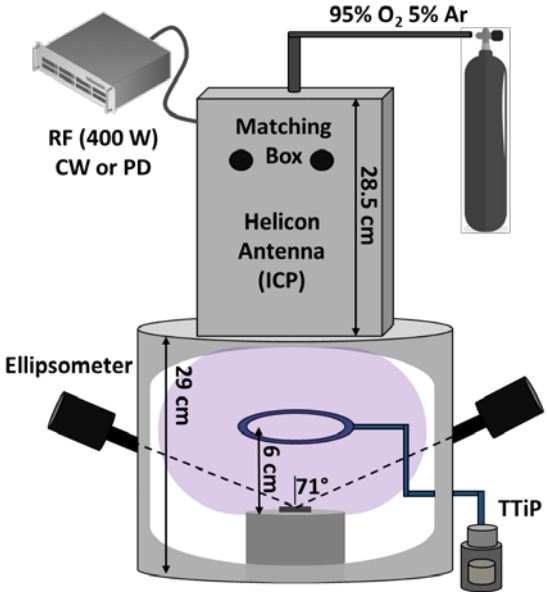

Figure 1 : Schematic of the experimental setup including the low-pressure ICP O_2 plasma source, the diffusion chamber and the Titanium precursor vapor injection system. The *in situ* ellipsometry apparatus is also indicated.

A flow rate of 24 sccm of O_2 including 5% Ar is injected from the top of the plasma source where the discharge is ignited and maintained. The oxygen plasma then diffuses in the deposition chamber underneath. Titanium(IV) Tetraisopropoxide ($Ti(OC_3H_7)_4$, TTiP, 99.999%, supplied by Sigma Aldrich Ltd.) was used as titanium precursor and was injected in the deposition chamber through a dispersal ring of 12 cm in diameter, placed 6 cm above substrate holder plate. The TTiP injection system (Nanosource, Omicron Technologies) is pressure regulated and ensures a stable TTiP vapor flowrate without carrier gas.

Two sets of deposition conditions were considered in this study: one in continuous-wave plasma discharge (CW) and one in pulsed plasma discharge (PD). In each set, film thicknesses of 80, 150, 250 and

450 nm were prepared, by adjusting the deposition time while monitoring by *in situ* spectroscopic ellipsometry was carried out during the deposition. Plasma discharge was pulsed with a frequency, f, of 1 kHz and a Duty Cycle, DC, of 50 %, which corresponds to a mean rf power of 200 W. With temperature-sensitive labels placed under the substrates, the temperature was shown to remain between 127 and 132°C in CW plasma mode, and between 77 and 82°C in pulsed plasma mode, regardless of the deposition time, in the investigated range of deposition times. The observed difference between the two modes is linked to the substrate heating resulting from the plasma surface interactions (recombination of oxygen atoms and ions on the film surface).

Samples characteristics are gathered in Table 1 and each sample is denoted XY, where X stands for the plasma condition (CW or PD) and Y for the targeted thickness in nm. One can note that, for the same precursor injection conditions, the deposition rate is slightly higher when pulsing the discharge compared to the continuous mode (1.6±0.1 nm min^{-1} versus 1.3±0.1 nm min^{-1}). For all deposits in a same discharge mode, the deposition rate was stable enough to ensure that microstructural changes with thickness depend on the growth mechanism only.

Table 1: Samples and deposition conditions

Sample	Deposition time (min)	Thickness (nm)		Deposition rate (nm min^{-1}) (±0.1)
		Ellipsometry (±2)	SEM cross section (±10)	
CW80	67	91	90	1.4
CW150	126	157	152	1.2
CW250	193	261	255	1.4
CW450	330	451	450	1.4
PD80	55	85	80	1.5
PD150	92	153	150	1.7
PD250	153	261	262	1.7
PD450	299	457	450	1.5

All the as-deposited TiO_2 thin films on Si were investigated by X-Ray Diffraction (XRD; Siemens D8 diffractometer) using the Cu Kα radiation at 40 kV, 40 mA, in the 22-80° 2θ range with a step of 0.03°. The

Lotgering method was used to measure the degree of orientation of the films.(40) This method compares the relative intensity, p_i, of a given reflection peak i ($p_i=I_i/\Sigma I_{hkl}$, with I_i and I_{hkl} the intensities of the i peak and (hkl) peaks respectively) to the relative intensity (p_0) of the same reflection peak for a randomly oriented sample ($p_0=I^0_i/\Sigma I^0_{hkl}$ with I^0_i and I^0_{hkl} the expected intensities of the i peak and (hkl) peaks respectively in a powder-like diffractogramm). Then for each peak of the pattern, the Lotgering factor f_i is calculated using the formula $f_i=(p_i-p_0)/(1-p_0)$.

The films surface and side-view morphology were observed by Scanning Electron Microscopy (SEM, JEOL-type JSM 7600F) operating at 5 kV in secondary electron mode. Atomic force microscopy (AFM) images were taken with a commercial instrument (Nanowizard II AFM, JPK Instruments AG, Berlin, Germany). The scanning was performed using the intermittent contact mode with nanosensor cantilevers PPP-NCH having a nominal force constant of about 42 N m^{-1} and resonance frequency of about 330 kHz. Exploitation was made using JPK Data Processing software. The growth was monitored by *in situ* spectroscopic ellipsometry using J.A. Woollam M-2000, at angle of incidence 71°, in the range 245-1000 nm. The ellipsometer apparatus used in this work uses rotating compensator ellipsometer technology along with CCD detection, allowing collecting the entire spectrum in a few seconds. The ellipsometric data were analyzed with the CompleteEASE software, v6.39. Finally, the photocatalytic activity of the as-deposited thin films on Si was investigated by measuring Methylene Blue (MB) decomposition in aqueous solution under UV illumination, by following the absorbance decrease by UV-Visible Spectroscopy (Tecan Infinite M1000 Pro). Prior to any UV illumination, the samples were immersed in the [MB] = 1 µmol L^{-1} solution then stored under dark condition for one night in order for the adsorption/desorption to reach equilibrium. The 365 nm UV lamps (Herolab UV-8 SL, 365 nm, 2x8 W) were then placed at a distance around 8 cm so the measured irradiance was set at 3 mW.cm^{-2}. (26,41)

3. Results and Discussion

3.1 Crystalline structure

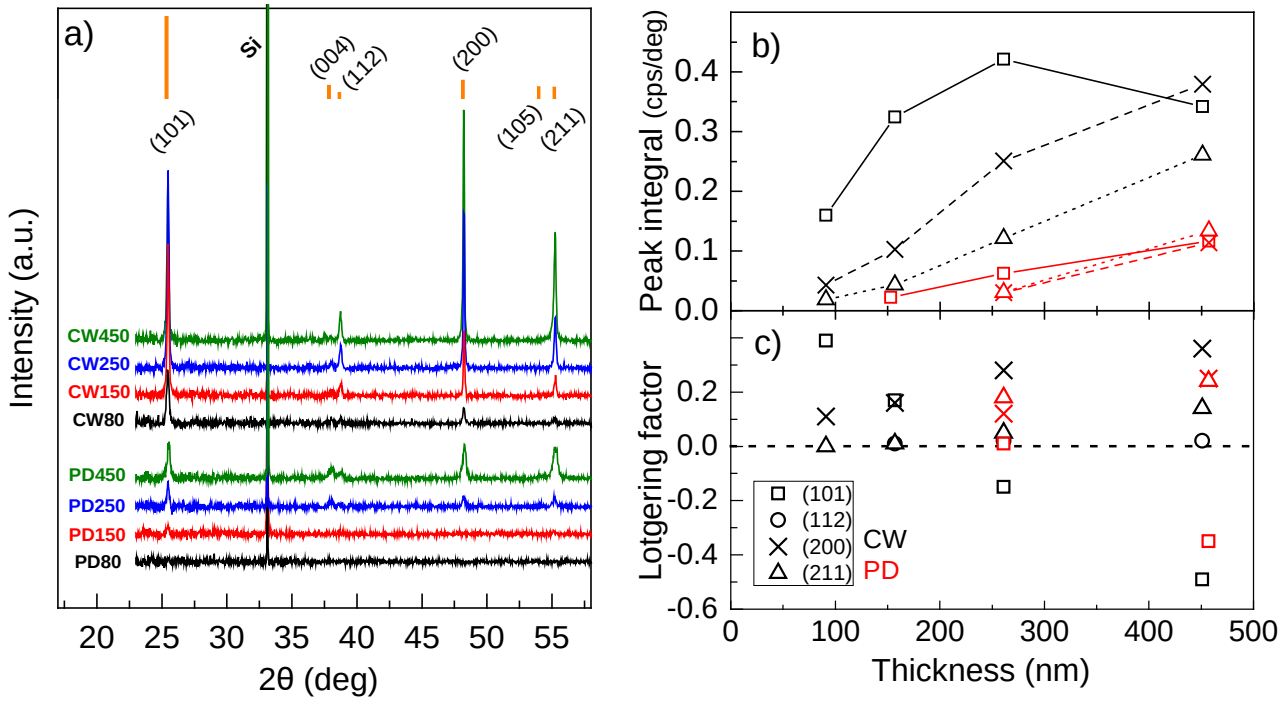

Figure 2 : a) XRD pattern of thin films deposited in CW plasma (top) and pulsed plasma (bottom) modes. Graphs are shifted in intensity for better reading. The expected pattern of a randomly oriented sample is plotted above as orange bars. b) Integrated intensities and c) Lotgering factors of crystallographic planes (101): squares, (112): circles, (200): crosses and (211): triangles in CW (black) and PD (red) plasma as a function of film thickness.

The X-ray diffraction patterns of all of the thin films deposited on Si are presented in Figure 2.a. The peaks of the anatase phase matching with the JCPDS file 89-4921 are shown in Fig 1.a as orange bars. Occasionally, the Si-(200) forbidden reflection appears at 33° depending on substrate orientation in the XRD apparatus. The integrated intensities of the main peaks and their Lotgering factors are displayed as a function of film thickness in Figure 2.b and c, respectively.

The XRD patterns of TiO_2 thin films deposited in CW plasma exhibit the peaks of the anatase phase. However, it has to be noticed that some of them are very low in intensity or even not detected at all such as (004) and (105), meaning that the films exhibit some preferential orientation. As can be seen in Figure 2.b, the integrated peak intensity increases for planes (200) and (211) with thin film growth. Surprisingly, the intensity of (101) peak decreases between 250 and 450 nm for continuous plasma deposition. This is explained by (101) planes not all being brought in diffraction condition in the focus plane of the diffractometer. This effect is typical when studying orientated films in Bragg-Brentano geometry, hence suggesting preferential growth. For CW80, a preferential orientation is found along (101) plane, with f_{101} =

0.39. When thickness increases, f_{101} decreases and even displays negative values after 150 nm. This may be interpreted as planes (101) being hindered but could also be due to aforementioned configuration limitations. In the meantime, crystallographic planes (200) and (211) appear to be favored by thickness, with increasing Lotgering factors. In contrast to these evolutions, (112) plane appears as randomly distributed, with f_{112} being close to zero whatever the film thickness.

Thin films deposited in pulsed discharge exhibit a slightly different behavior. Up to a thickness of 150 nm (sample PD150), the thin film appears mainly amorphous. The peak corresponding to (101) crystallographic plane is visible, though poorly defined, at 150 nm. Anatase only clearly appears for PD250 and PD450, with the same visible peaks as in continuous plasma discharge. This feature is coherent with the gradual crystallization of anatase along the growth direction previously evidenced by SAED.(26) Preferential orientation similar to the CW films is observed, with crystallographic planes (200) and (211) being favored at the highest thickness (f_{200} = 0.25 and f_{211} = 0.24) while (101) appears as hindered with negative f_{101}. It is thus clear that thickness plays a key role for the apparition of anatase in Pulsed-PECVD. Despite lower deposition temperature, this demonstrates that anatase growth is possible in this mode provided that sufficient thickness is reached.

3.2 Morphology

Side-view SEM micrographs of the 450 nm thick films deposited in CW and PD modes are displayed in Figure 3. They reveal the expected columnar morphology for both conditions, in agreement with previous results.(26) One can observe a first layer of dense thin columns turning into a second layer with larger columns. The transition thickness, defined as the thickness corresponding to the transition between thin and larger columns, is shifted from approximately 135-150 nm to 200-250 nm when going from CW to PD deposition.

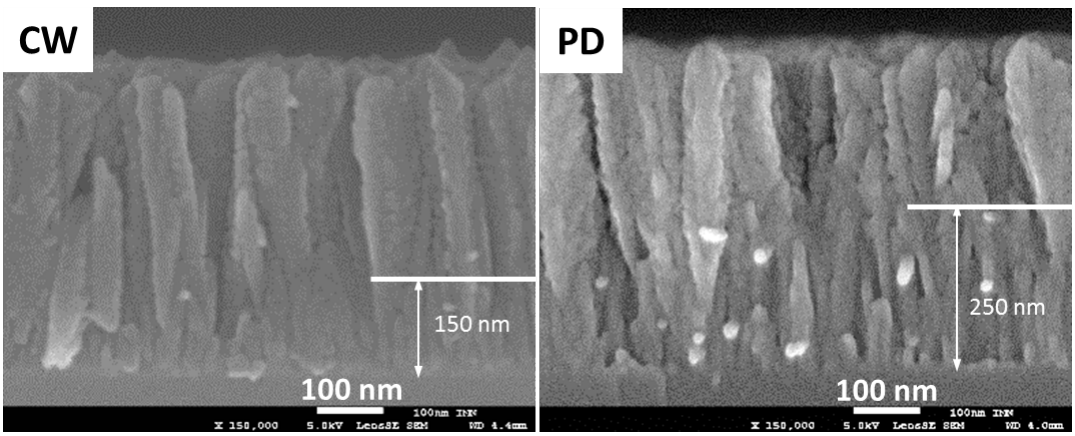

Figure 3 : SEM picture, x150 000, of the cross-section of 450 nm thin films deposited in (left) continuous-wave plasma mode and (right) pulsed plasma mode. White segment indicates the transition thickness between dense thin columns and larger columns

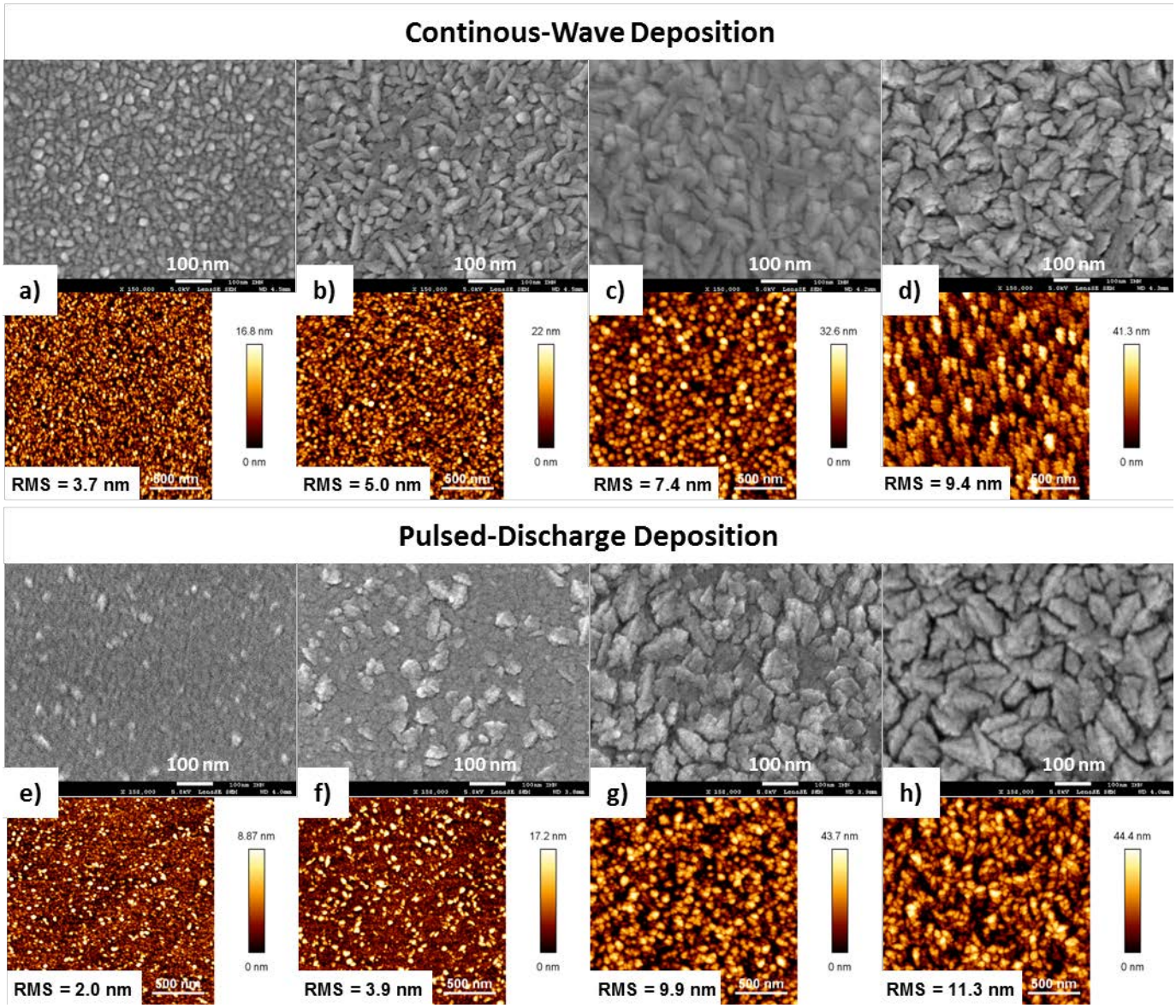

Figure 4 : SEM, x150 000, and AFM, 2 µm x2 µm, images of the top surface of thin films deposited in (top) continuous-wave plasma mode or (bottom) pulsed plasma mode, at thickness (a, e) 80 nm, (b, f) 150 nm, (c, g) 250 nm and (d, h) 450 nm. Scale bars correspond to 100 nm and 500 nm for SEM and AFM micrographs, respectively. The root mean square mean deviation (RMS) is used to quantify roughness, based on these 2 µm x 2 µm images and additional 1 µm x 1 µm images.

Top-views of the two sets of TiO_2 thin films are shown in Figure 4, from SEM and AFM analyses. For all deposits, bright contrast grains can be observed on the surface of SEM images, matching with the bright grains detected by AFM. They very likely correspond to the tip of large columns protruding from the surface, with sharp endings inducing roughness and thus exhibiting charging effects in SEM.(33) On PD80 and PD150 samples especially (see Figure 4.e and 3.f), a homogeneous darker contrast can be observed between bright columns, corresponding to the smoothest assembly of surrounding narrow columns.(26,29) Based on XRD results, previous works and literature, we can assume that the bright column ends are associated with crystallization of the film, while the darker contrast can be associated with amorphous-like TiO_2.(19,29,33,41) The column size is expected to be much larger than the crystal size, hence the use of the term "polycrystalline columns" through the article. Top-view SEM pictures have been exploited with ImageJ software to extract the density and average area of bright columns arising at the surface and the results are plotted in Figure 5.

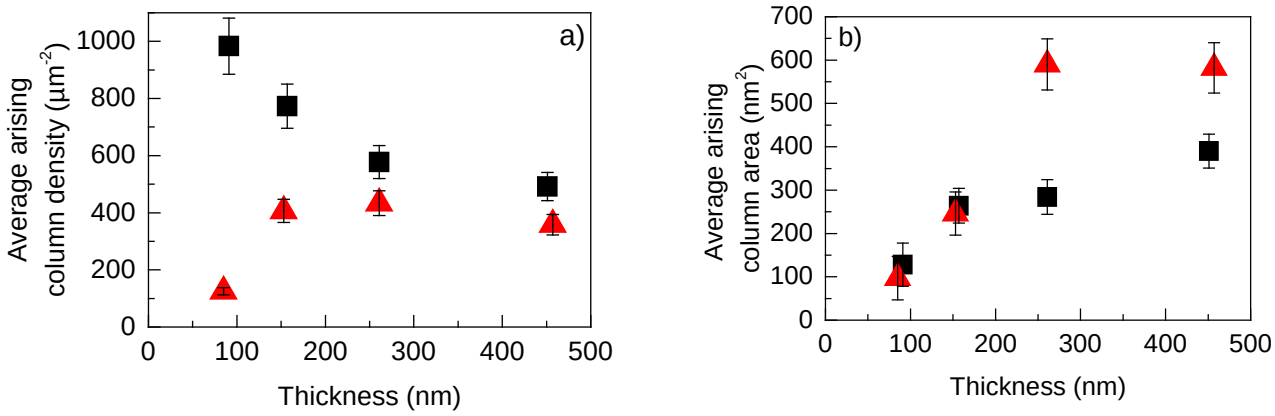

Figure 5 : a) Average density and b) Average area of anatase polycrystalline columns arising at surface as observed in top-view scanning electron microscopy for thin films deposited in continuous plasma (black squares) and pulsed plasma (red triangles)

For CW deposition, bright arising columns already cover the totality of the surface when the film thickness is 80 nm only, with numerous columns of 128 nm^2 in average area. Further growth shows decreasing column density from 983 μm^{-2} to 492 μm^{-2} and increasing column area up to 390 nm^2, which indicates that a strong competition occurs perpendicularly to the growth direction. This is associated with an increase in RMS roughness measured by AFM from 3.7 nm for CW80 to 9.4 nm for CW450.

In pulsed discharge deposition, several bright columns can be observed when the achieved thickness is 80 and 150 nm, with increasing density (125 and 406 μm^{-2}, respectively) and average area (97

and 246 nm^2, respectively). Considering that these columns can be linked to crystallized TiO_2, this suggests that some anatase already appears at the first steps of growth, below 150 nm, even if no anatase peak is detected by XRD in the case of PD80. This is very likely related to the small dimensions of crystalline domains. Between PD80 and PD150, the films have a low and slowly increasing RMS roughness of 2.0 and 3.9 nm respectively, as determined by AFM, which is consistent with the low density of columns arising at the surface. When the thickness increases, new grains appear, larger columns develop, and narrow columns are gradually capped. The density of bright columns increases up to 433 μm^{-2}, very close to the value reached in CW mode. Their average area at the surface of the film increases up to 590 nm^2 for PD250. For further growth (PD450), the density of columns decreases (358 μm^{-2}) and stabilization of their average area (582 nm^2) is observed. The RMS roughness is strongly enhanced to 9.9 and 11.3 nm for PD250 and PD450, respectively. These values are even higher than that of CW250 and CW450, suggesting strong effect of the size of polycrystalline grains. The stabilization of both average area and roughness suggests that a competitive growth has taken place, with "coalescence" of polycrystalline columns happening between 250 and 450 nm. The difference in average area of arising columns between CW and PD mode for films thicker than 150 nm, with PD columns being up to twice as big as CW columns, may be related to the lower density of polycrystalline grains, acting as column nucleation sites, in the initial steps of the growth. Indeed, lower column density induces less lateral competition for the V-shape growing columns and delays the columns critical thickness of coalescence.(23,37,42)

3.3 In situ Spectroscopic Ellipsometry

All depositions were monitored by *in situ* spectroscopic ellipsometry. The ellipsometric data (spectra recorded every 3 s) can be analyzed in two ways: kinetic or spectroscopic. Kinetic ellipsometry consists in analyzing the evolution of ellipsometric parameters Ψ and Δ with time, at a fixed wavelength. One can also use I_N, I_s and I_c parameters, which are related to Ψ and Δ by Eq.1, Eq.2 and Eq.3, respectively. This analysis of I_s and I_c parameters is independent of a model and thus displays direct experimental information on the growing film. If the thin film is transparent at the observation wavelength (k_λ=0) and homogeneous along the growth direction, the ellipsometric trajectory for a given wavelength is periodic as a function of time and I_s versus I_c curves exhibit cyclic trajectories.(43) At fixed wavelength λ and angle of incidence Φ, one trajectory cycle corresponds to a specific thickness , denoted hereafter period thickness d, depending only on the refractive index of the thin film grown, n, according to Eq.4.

$$I_N = \cos 2\Psi \qquad \text{Eq.1}$$

$$I_S = \sin 2\Psi \sin \Delta \qquad \text{Eq.2}$$

$$I_C = \sin 2\Psi \cos \Delta \qquad \text{Eq.3}$$

$$d = \frac{\lambda}{2\sqrt{n^2 - \sin^2 \Phi}} \qquad \text{Eq.4}$$

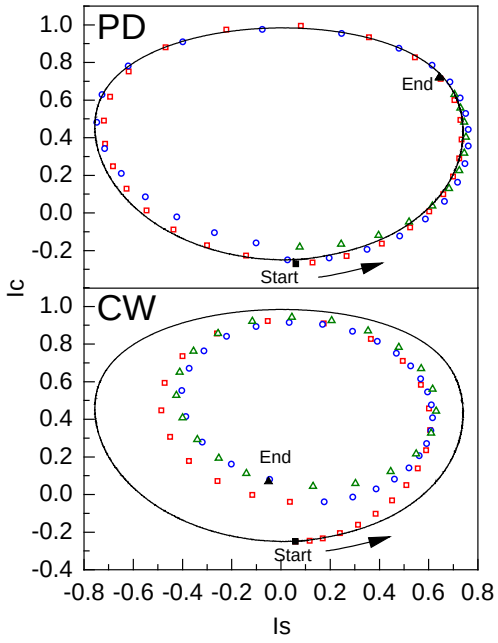

Figure 6 : Ellipsometric trajectories of PD450 (top) and CW450 (bottom) growths at 633nm. Open red squares, first period; open blue circles, second period; open green triangles, third period. The simulated periodic trajectory of a homogeneous TiO_2 thin film, of n@633nm=2.0, is shown as a line. Arrows show the evolution with time.

Ellipsometric trajectories (Is-Ic, at λ=633nm) of 450 nm thick films grown in continuous and pulsed plasma are displayed in Figure 6. In order to provide a reference, the simulated ellipsometric trajectory of a homogeneous thin film of refractive index n=2.0, is featured. The corresponding period thickness is 180 nm.

In pulsed plasma deposition (Figure 5 top), the trajectory is almost cyclic indicating that the film growth is homogeneous-like. The first trace is well superimposed with the reference one and optical index value n=2.0 can be assumed. At the end of the second cycle, the ellipsometric trajectory starts to shift aside, consistently with heterogeneities appearance. The transition occurs when the thickness evolves between 200 and 300 nm, which is consistent with the observations from SEM cross-view images.

For CW plasma deposition (Figure 5 bottom), the ellipsometric trajectory shifts aside the reference data shortly after the start of the deposition. The second trace is still shifted whereas the third one is very close to the second one. The quasi-periodic optical thickness estimated from Eq.4 (assuming homogeneous growth) on the final cycles appears smaller than reference one, which indicates an increase of the refractive index. Both the increase of the refractive index and the change of the kinetic trajectory from the first tens of nanometers of the growth, are consistent with anatase domains formation in the early stages of the growth.

Hence, kinetic ellipsometry at a fixed wavelength evidences a different behavior for thin films growth depending on the plasma discharge mode. It however remains limited to a quality indicator for a given growth process. For further insights, and to determine the layer thickness and optical properties, spectroscopic data have been analyzed for all samples at the end of deposition. The stacking used for spectroscopic ellipsometry data modeling is presented in Figure 7 (Left).

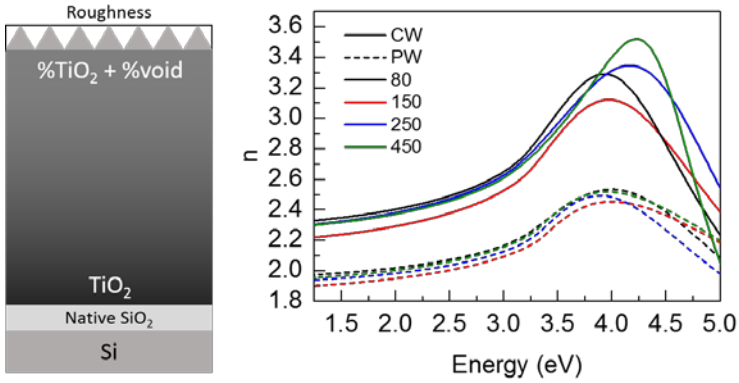

Figure 7 : (Left) Schematic layer stacking used to describe the thin film deposited on the Si substrate. (Right) Refractive index of the TiO_2 material without void versus the photon energy: CW mode shown as full lines and PD mode as dashed lines

It is composed of three layers on a Si substrate: 1) native SiO_2 layer (2 to 3 nm), 2) TiO_2 layer and 3) Roughness layer. The roughness layer is modeled as a 50% TiO_2 and 50% void mixed material, with Bruggeman Effective Medium Approximation (BEMA). The TiO_2 layer is constructed as a 20-step gradient layer ($1 \leq i \leq 20$), each being $1/20^{th}$ of the total layer thickness, and mixing TiO_2 and voids with BEMA. The fraction of voids is set at zero at the bottom and is fitted at the top of the TiO_2 layer ($void_{top}$). The void fraction in each sub layer varies linearly with the TiO_2 layer thickness, such that sub-layer i void percentage is defined as $void_{top}*i/20$. TiO_2 optical constants are modeled with a Tauc-Lorentz oscillator (TL), which is Kramers-Kronig consistent, accordingly to previous works.(44) This stacking was found as the most

accurate to describe thin films for both continuous and pulsed discharge deposition, at any given thickness included in the range of this study. The parameters adjusted to fit the calculated data to the experimental data are: TiO_2 TL optical constants, top void fraction, TiO_2 layer thickness and top Roughness layer thickness. The data acquisition and fit were performed at the end of the growth process to later provide comparison with in-growth measurements.(45) The quality of the fit was monitored with the Mean Squared Error (MSE), calculated using Eq.5, where *w* is the number of wavelengths and *m* is the number of fitted parameters. MSE is notably sensitive to the roughness of the film that enhances diffusion of light at the surface, deviating the analysis from specular conditions. Despite seemingly high MSE, especially at high thickness, the uniqueness of the solution is observed whatever the initial set of parameters. Results of the fits are displayed in Table 2.

$$MSE = \sqrt{\frac{1}{3w-m}\sum_{i=1}^{n}\left[\left(\frac{I_{N_i}^{mod}-I_{N_i}^{exp}}{0.001}\right)^2+\left(\frac{I_{C_i}^{mod}-I_{C_i}^{exp}}{0.001}\right)^2+\left(\frac{I_{S_i}^{mod}-I_{S_i}^{exp}}{0.001}\right)^2\right]} \qquad \text{Eq.5}$$

Table 2: Spectroscopic Ellipsometry results for all the deposited films

Sample	Film Thickness (nm) (±3)	Roughness layer thickness (nm) (± 1)	n @633nm of TiO_2 material (± 0.1)	E_g of TiO_2 material (eV) (± 0.1)	MSE
CW80	91	5	2.5	3.2	10
CW150	157	17	2.3	3.1	30
CW250	257	23	2.4	3.0	34
CW450	451	30	2.4	3.0	45
PD80	85	4	2.1	3.2	16
PD150	153	13	1.9	3.3	38
PD250	261	31	2.0	3.3	58
PD450	457	37	2.0	3.3	101

For all the deposited films the thicknesses of the TiO_2 layer determined from ellipsometry and SEM (reported in Table 1) are very close. The TiO_2 refractive index is systematically higher (n=2.4 at 633 nm) for

the films deposited in CW plasma than for those deposited in pulsed plasma (n=2.0), which reflects their better overall crystallization, in agreement with XRD and kinetic ellipsometry results. By plotting the refractive indices over the whole spectral range of the fit, as shown in Figure 6 (Right), we observe that the optical index at low photon energy is rather similar for samples of a given deposition mode, with the important increase in value (~+ 0.4) when going from PD to CW mode. However, more pronounced discrepancies are observed on the real part of the optical index in the 4-5 eV photon range. This is likely due to the fact that optical diffusion effects, which are mainly governed by the columnar morphology and top film roughness, are more pronounced at short wavelengths (see Table 2). In addition, the optical band gap as modeled by spectroscopic ellipsometry is found to decrease for samples prepared in CW mode, from 3.2 to 3.0 eV with increasing thickness, and rather stable at 3.3 eV for samples obtained in PD mode. Decreasing of the optical band gap of TiO_2 thin films might be correlated to increasing anatase crystallization or size of anatase nanocrystallites, due to the evolution of film morphology.(46,47)

The roughness determined by spectroscopic ellipsometry is a simulated roughness layer thickness derived from an optical model, hence is not a direct surface roughness value. As can be seen in RENVOI, it varies linearly with AFM RMS roughness. The higher values deduced from ellipsometric measurements can be explained considering the different calculation modes. These results allow validating the use of ellipsometry for the roughness accurate determination, independently of the deposition process.

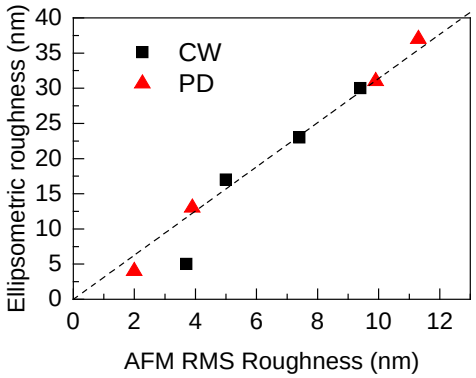

Figure 8 : LEGEND

The values of Ψ and Δ were recorded *in situ* over the whole spectral range with an acquisition time of 1 s and an analysis every 3 s. As the growth rate is in the order of 1 nm min^{-1}, the film thickness can be considered to be constant for one full spectrum acquisition time. This sampling time measurement allows a continuous-like monitoring. This allows for spectroscopic modeling at any deposition stage, which appears

as a very powerful tool. Thin films growth can thus be monitored with high precision and parameters such as thickness and roughness can be easily determined, overcoming the issues encountered with the classic kinetic measurement at one wavelength.(48,49)

In this perspective, spectroscopic modeling has been carried out all along the growth of CW450 and PD450 samples, with the same stacking as in Figure 6 (Left). Figure 9 displays the fitted roughness against the fitted thickness of the films during deposition. Fits under 70 nm are not presented due to the correlation between thickness, top void fraction and roughness at low thicknesses.

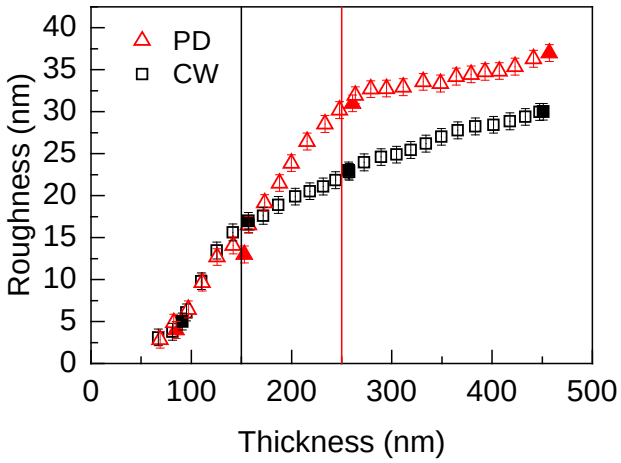

Figure 9 : Roughness layer thickness as a function of film thickness in CW plasma deposition (black squares) and pulsed plasma deposition (red triangles) as measured by ellipsometry during the film growth (open symbols) and after the growth (full symbols)

~~*The roughness deduced from ellipsometry is found to increase with thickness, consistently with SEM observations and AFM measurements.*~~(19,30)~~*One can note the differences in ellipsometric roughness between samples of same thickness: up to 150 nm, the ellipsometric roughness is slightly higher in continuous plasma than in pulsed plasma deposited films, whereas beyond 150 nm the trend is reversed, consistently with AFM observations. As both AFM and ellipsometric roughness appears dependent of the polycrystalline columns presence at the surface of the film, this suggests that this parameter could be used to monitor the growth mechanism.*~~

The analysis of the ellipsometric data measured *in situ* during the growth of the thick films can be considered representative of all other samples, as perfect consistency is found with thinner films. For both

CW and PD modes, the roughness layer thickness increases with film thickness, as expected from the analysis of each sample. It appears however that in the two plasma conditions the increase in roughness with thickness exhibits two regimes: a rapid increase followed by a much slower one. Indeed both curves are superimposed, thus independent of the plasma mode. In this first regime, the roughness evolution is given by Roughness(nm) = (Film thickness(nm)-70)×0.16+2.8, based on a linear regression. In the second regime, the slope is found to be lowered by a factor more than 4, whatever the discharge mode operation (CW or PD). The transition between the two steps appears at different thicknesses depending on the discharge mode: at 150 nm for continuous mode and 250 nm for pulsed mode. This transition in the roughness evolution may be linked to the coalescence of polycrystalline columns, which can no longer develop laterally, and hence corresponds to the critical transition thickness. The first regime thus reflects the growth of sharp polycrystalline columns in a matrix of thin columns, while the second regime represents the competitive growth of the large columns.

3.4 Photocatalytic properties

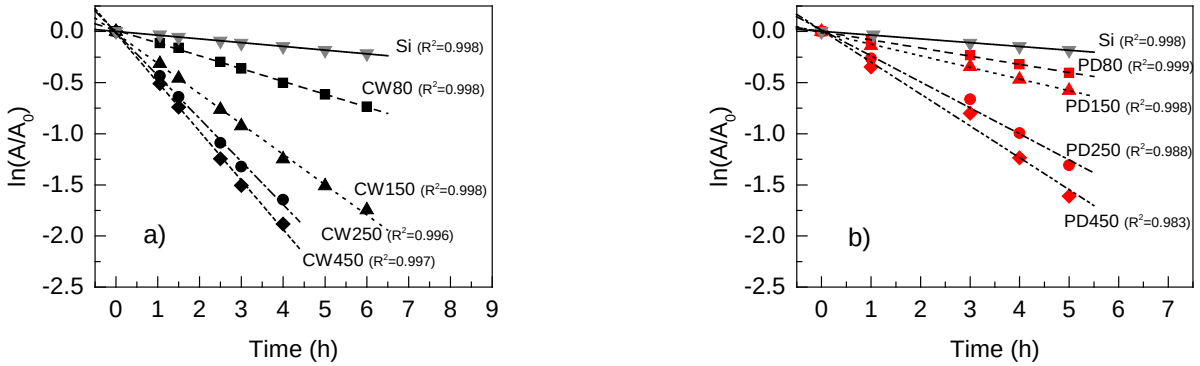

Figure 10 : Photodegradation kinetics of Methylene Blue in presence of a) TiO_2 thin films deposited in continuous plasma conditions (the points at 5 and 6 hours are not shown for CW250 and CW450 samples because Methylene Blue reactant had been fully consumed) or b) TiO_2 thin films deposited in pulsed plasma conditions

The photocatalytic activity of thin films has been approached by measuring Methylene Blue [MB] decomposition under UV exposure. UV-Visible Spectroscopy was used to monitor the decrease in dye concentration in the aqueous solution, following the absorbance maximum at 664 nm. The photodegradation kinetics of MB by continuous and pulsed plasma deposited TiO_2 thin films are presented in Figure 10.a) and Figure 8.b), respectively. If a Langmuir-Hinshelwood model should be considered to

respect true photocatalytic kinetics, we will here approximate the reaction with a first order kinetics. Indeed, for all films the MB absorbance decreases as a function of UV exposure time following an exponential law, $A=A_0 \times \exp(-kt)$, A_0 being the initial absorbance of MB aqueous solution, k the apparent degradation reaction constant and t the UV exposure time. In a first approximation, the kinetics of the degradation process can thus be given as a first order reaction, $\ln(A/A_0)=-kt$, where k can be determined by a linear fit of a $\ln(A/A_0)$ versus t plot.

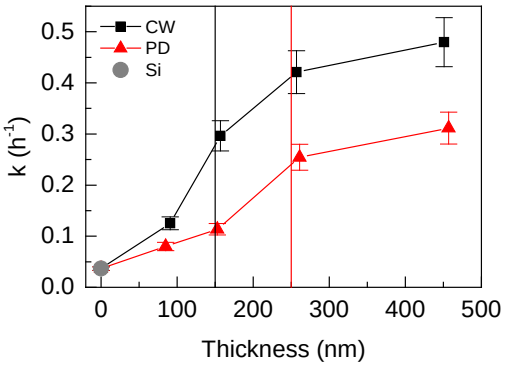

Figure 11 : Photocatalytic degradation reaction constant k as a function of film thickness and plasma mode. Black squares: CW. Red triangles: PD. Grey circle: silicon substrate. Black and red bars, critical thicknesses in CW and PD mode.

As presented in Figure 11, all the samples are photocatalytically active since the reaction constant k is higher than for the Si substrate reference. Whatever the thickness in the studied range, the film deposited in pulsed plasma mode is less photocatalytic than the one deposited in continuous plasma, consistently with what was previously observed for 300 nm thick films.(26) As the photocatalytic activity of the thin film can be directly related to the crystallinity of the TiO_2 material, this is consistent with XRD and SEM results. (50,51) It is especially interesting to link the photocatalytic properties evolution to the critical thickness derived from the dynamic *in situ* spectroscopic ellipsometry analysis. Indeed, a photocatalytic activity breakthrough is observed when this specific thickness is reached for each deposition mode. The photocatalytic activity is greatly increased between 80 and 150 nm for CW and between 150 and 250 nm for PD. Further growth does not impact so significantly the photocatalytic properties, consistently with the lower evolution of the roughness. This behavior at high thickness might also be a hint that only the upper part of the film plays a role in the photocatalytic process, which would likely be due to the Methylene Blue not penetrating the thin film down to the substrate. The thickness of coalescence defined from dynamic *in*

situ spectroscopic ellipsometry analysis therefore corresponds to the critical thickness for photoactivity discussed in the literature.(38) This key parameter for photocatalytic applications can thus be measured using a single deposition experiment, for a given set of process conditions.

3.5 Growth mechanism

Ultimately, continuous and pulsed plasma deposited TiO_2 thin films appear to share similar growth mechanism, as illustrated in Figure 12. In the first deposition sequence (1), the film contains nanosized domains, already crystallized, that subsequently (2) grow into columns according to the Kolmogorov model. The critical thickness corresponds to the one at which these V-shaped polycrystalline columns coalesce in a thin columns matrix (3) and induce their competitive growth for greater thicknesses (4).

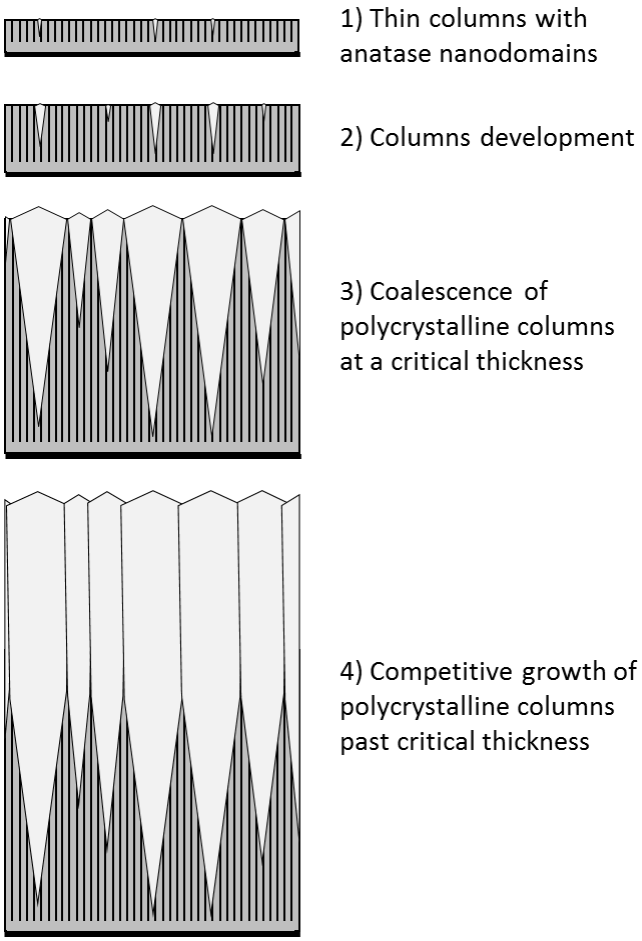

Figure 12 : Schematic illustration of the polycrystalline columns coalescence phenomenon

This coalescence appears as a critical step for the growth mechanism of crystallized TiO_2 at low temperature by PECVD, directly impacting morphology and photocatalytic properties. This value could be used as a monitoring parameter to compare the impact of process conditions on the growth. In pulsed discharge, the amount of crystallized domains in the first layer is less than for the CW mode, which consequently delays the critical thickness appearance. This phenomenon evidences a relationship between the value of this critical thickness and the deposition process conditions: with less energy transferred to the growing material in the case of the pulsed discharge, the corresponding critical thickness is increased. A thicker film is then required to achieve similar photocatalytic properties. This could be due to pure thermal effects(8) or reduction of the active deposition species energy.(32) It should also be noted that the temperature at the top surface of the growing film exposed to the plasma might locally be far higher than the values measured at the back of the substrate. The impact of the plasma off-times should also not be neglected and further studies on the plasma-surface interactions are needed. Furthermore, additional work would be useful to determine the relationship between the coalescence thickness and different parameters, such as the plasma composition, the discharge power and the deposition rate for example.

4. Conclusion

TiO_2 thin films were deposited by low-temperature PECVD and Pulsed-PECVD using O_2 and TTiP precursor. Their morphology, structure and photocatalytic properties were investigated as a function of their thickness (80-450 nm) with the valuable input of the spectroscopic ellipsometry data recorded *in situ* all along the film growth. All the films deposited at 130°C in continuous-wave plasma exhibit the anatase phase, with high refractive index, whereas films deposited in pulsed discharge at 80°C show gradual crystallization and lower refractive index. It has been shown that the photocatalytic activity is very dependent on the film thickness. The enhancement of photocatalytic activity is attributed to a cumulated effect of crystallization and roughness increase with film thickness. A breakthrough is found for a critical thickness, which has been determined by dynamic *in situ* spectroscopic ellipsometry analysis based on the evolution of the film top roughness as a function of its thickness. This critical thickness is dependent on the growth mechanism and has been estimated at about 150 nm for CW and 250 nm for PD deposited samples. For each deposition condition, it is associated with the transition from small size to large size coalesced columns, in good agreement with the SEM, AFM and XRD investigations.

Acknowledgments

The authors gratefully acknowledge the financial support of the French Agence Nationale de la Recherche (ANR) and Luxembourgish Fonds National de la Recherche (FNR) through the FNR-ANR-INTER project PATIO (ANR-17-CE08-0045-01 and INTER/ANR/16/11565003/PATIO/Choquet).

References

1. Nozik AJ. Photochemical diodes. Appl Phys Lett. 1 juin 1977;30(11):567‑9.
2. Teichner SJ. The origins of photocatalysis. J Porous Mater. 1 juin 2008;15(3):311‑4.
3. Henderson MA. A surface science perspective on TiO2 photocatalysis. Surf Sci Rep. 15 juin 2011;66(6):185‑297.
4. Yanagisawa K, Ovenstone J. Crystallization of Anatase from Amorphous Titania Using the Hydrothermal Technique: Effects of Starting Material and Temperature. J Phys Chem B. 1 sept 1999;103(37):7781‑7.
5. Pore V, Rahtu A, Leskelä M, Ritala M, Sajavaara T, Keinonen J. Atomic Layer Deposition of Photocatalytic TiO2 Thin Films from Titanium Tetramethoxide and Water. Chem Vap Depos. 2004;10(3):143‑8.
6. Shan G-B, Demopoulos GP. The synthesis of aqueous-dispersible anatase TiO2nanoplatelets. Nanotechnology. déc 2009;21(2):025604.
7. Reyes-Coronado D, Rodríguez-Gattorno G, Espinosa-Pesqueira ME, Cab C, Coss R de, Oskam G. Phase-pure TiO2nanoparticles: anatase, brookite and rutile. Nanotechnology. mars 2008;19(14):145605.
8. Hodgkinson JL, Yates HM, Sheel DW. Low Temperature Growth of Photoactive Titania by Atmospheric Pressure Plasma: Low Temperature Growth of Photoactive Titania by …. Plasma Process Polym. 15 sept 2009;6(9):575‑82.
9. Lee C-S, Kim J, Son JY, Choi W, Kim H. Photocatalytic functional coatings of TiO2 thin films on polymer substrate by plasma enhanced atomic layer deposition. Appl Catal B Environ. sept 2009;91(3‑4):628‑33.
10. Horikoshi S, Serpone N. Can the photocatalyst TiO2 be incorporated into a wastewater treatment method? Background and prospects. Catal Today. janv 2020;340:334‑46.
11. Leyva-Porras C, Toxqui-Teran A, Vega-Becerra O, Miki-Yoshida M, Rojas-Villalobos M, García-Guaderrama M, et al. Low-temperature synthesis and characterization of anatase TiO2 nanoparticles by an acid assisted sol–gel method. J Alloys Compd. 25 oct 2015;647:627‑36.
12. Jolivet J-P, Cassaignon S, Chanéac C, Chiche D, Tronc E. Design of oxide nanoparticles by aqueous chemistry. J Sol-Gel Sci Technol. 1 juin 2008;46(3):299‑305.
13. Karpinski A, Berson S, Terrisse H, Mancini-Le Granvalet M, Guillerez S, Brohan L, et al. Anatase colloidal solutions suitable for inkjet printing: Enhancing lifetime of hybrid organic solar cells. Sol Energy Mater Sol Cells. 1 sept 2013;116:27‑33.
14. Kelly PJ, Barker PM, Ostovarpour S, Ratova M, West GT, Iordanova I, et al. Deposition of photocatalytic titania coatings on polymeric substrates by HiPIMS. Vacuum. juill 2012;86(12):1880‑2.
15. Ratova M, West GT, Kelly PJ. Optimisation of HiPIMS photocatalytic titania coatings for low temperature deposition. Surf Coat Technol. 15 juill 2014;250:7‑13.

16. Kääriäinen TO, Kelly PJ, Cameron DC, Beake B, Li H, Barker PM, et al. Nanoscratch testing of atomic layer deposition and magnetron sputtered TiO2 and Al2O3 coatings on polymeric substrates. J Vac Sci Technol Vac Surf Films. janv 2012;30(1):01A132.
17. Kubala NG, Rowlette PC, Wolden CA. Plasma-Enhanced Atomic Layer Deposition of Anatase TiO2 Using TiCl4. J Phys Chem C. 17 sept 2009;113(37):16307‑10.
18. Jeong HY, Kim YI, Lee JY, Choi S-Y. A low-temperature-grown TiO_2 -based device for the flexible stacked RRAM application. Nanotechnology. 19 mars 2010;21(11):115203.
19. Lee WG, Woo SI, Kim JC, Choi SH, Oh KH. Preparation and properties of amorphous TiO2 thin films by plasma enhanced chemical vapor deposition. Thin Solid Films. 1 janv 1994;237(1):105‑11.
20. Battiston GA, Gerbasi R, Gregori A, Porchia M, Cattarin S, Rizzi GA. PECVD of amorphous TiO2 thin films: effect of growth temperature and plasma gas composition. Thin Solid Films. 1 août 2000;371(1):126‑31.
21. Nakamura M, Korzec D, Aoki T, Engemann J, Hatanaka Y. Characterization of TiOx film prepared by plasma enhanced chemical vapor deposition using a multi-jet hollow cathode plasma source. Appl Surf Sci. 15 mai 2001;175‑176:697‑702.
22. Nakamura M, Kato S, Aoki T, Sirghi L, Hatanaka Y. Formation mechanism for TiOx thin film obtained by remote plasma enhanced chemical vapor deposition in H2–O2 mixture gas plasma. Thin Solid Films. 17 déc 2001;401(1):138‑44.
23. Ratzsch S, Kley E-B, Tünnermann A, Szeghalmi A. Influence of the oxygen plasma parameters on the atomic layer deposition of titanium dioxide. Nanotechnology. déc 2014;26(2):024003.
24. Kubala NG, Rowlette PC, Wolden CA. Self-Limiting Deposition of Anatase TiO2 at Low Temperature by Pulsed PECVD. Electrochem Solid-State Lett. 7 janv 2009;12(7):H259‑62.
25. Li D, Goullet A, Carette M, Granier A, Zhang Y, Landesman JP. Structural and optical properties of RF-biased PECVD TiO2 thin films deposited in an O2/TTIP helicon reactor. Vacuum. 1 sept 2016;131:231‑9.
26. Li D, Gautier N, Dey B, Bulou S, Richard-Plouet M, Ravisy W, et al. TEM analysis of photocatalytic TiO2 thin films deposited on polymer substrates by low-temperature ICP-PECVD. Appl Surf Sci. 15 oct 2019;491:116‑22.
27. Sobczyk-Guzenda A, Gazicki-Lipman M, Szymanowski H, Kowalski J, Wojciechowski P, Halamus T, et al. Characterization of thin TiO2 films prepared by plasma enhanced chemical vapour deposition for optical and photocatalytic applications. Thin Solid Films. 31 juill 2009;517(18):5409‑14.
28. Sobczyk-Guzenda A, Owczarek S, Szymanowski H, Gazicki-Lipman M. Amorphous and crystalline TiO2 coatings synthesized with the RF PECVD technique from metalorganic precursor. Vacuum. 1 juill 2015;117:104‑11.
29. Li D, Bulou S, Gautier N, Elisabeth S, Goullet A, Richard-Plouet M, et al. Nanostructure and photocatalytic properties of TiO2 films deposited at low temperature by pulsed PECVD. Appl Surf Sci. 1 févr 2019;466:63‑9.
30. Borrás A, Sánchez-Valencia JR, Garrido-Molinero J, Barranco A, González-Elipe AR. Porosity and microstructure of plasma deposited TiO2 thin films. Microporous Mesoporous Mater. 1 févr 2009;118(1):314‑24.
31. Borras A, Alvarez R, Sanchez-Valencia JR, Ferrer J, Gonzalez-Elipe AR. Critical thickness and nanoporosity of TiO2 optical thin films. Microporous Mesoporous Mater. 15 sept 2012;160:1‑9.
32. Ohring M. Materials science of thin films: deposition and structure. 2nd ed. San Diego, CA: Academic Press; 2002. 794 p.

33. Borras A, Sanchez-Valencia JR, Widmer R, Rico VJ, Justo A, Gonzalez-Elipe AR. Growth of Crystalline TiO2 by Plasma Enhanced Chemical Vapor Deposition. Cryst Growth Des. 3 juin 2009;9(6):2868‑76.
34. Borrás A, Cotrino J, González-Elipe AR. Type of Plasmas and Microstructures of TiO2 Thin Films Prepared by Plasma Enhanced Chemical Vapor Deposition. J Electrochem Soc. 2007;154(12):152‑7.
35. Maeda M, Watanabe T. Evaluation of photocatalytic properties of titanium oxide films prepared by plasma-enhanced chemical vapor deposition. Thin Solid Films. oct 2005;489(1‑2):320‑4.
36. Adamik M, Barna PB, Tomov I. Columnar structures in polycrystalline thin films developed by competitive growth. Thin Solid Films. 1 avr 1998;317(1):64‑8.
37. Lee W-J, Hon M-H. Space-Limited Crystal Growth Mechanism of TiO2 Films by Atomic Layer Deposition. J Phys Chem C. 22 avr 2010;114(15):6917‑21.
38. Jung S-C, Kim S-J, Imaishi N, Cho Y-I. Effect of TiO2 thin film thickness and specific surface area by low-pressure metal–organic chemical vapor deposition on photocatalytic activities. Appl Catal B Environ. 25 févr 2005;55(4):253‑7.
39. Granier A, Nicolazo F, Vallée C, Goullet A, Turban G, Grolleau B. Diagnostics in helicon plasmas for deposition. Plasma Sources Sci Technol. 1997;6(2):147.
40. Lotgering FK. Topotactical reactions with ferrimagnetic oxides having hexagonal crystal structures—I. J Inorg Nucl Chem. févr 1959;9(2):113‑23.
41. Dey B, Bulou S, Gaulain T, Ravisy W, Richard-Plouet M, Goullet A, et al. Anatase TiO 2 deposited at low temperature by pulsing an electron cyclotron wave resonance plasma source. Sci Rep. 15 déc 2020;10(1):1‑11.
42. Profijt HB, van de Sanden MCM, Kessels WMM. Substrate Biasing during Plasma-Assisted ALD for Crystalline Phase-Control of TiO2 Thin Films. Electrochem Solid-State Lett. 1 janv 2011;15(2):G1‑3.
43. Tompkins HG. A user's guide to ellipsometry. Boston: Academic Press, Inc; 1993. 260 p.
44. Li D, Carette M, Granier A, Landesman JP, Goullet A. Spectroscopic ellipsometry analysis of TiO2 films deposited by plasma enhanced chemical vapor deposition in oxygen/titanium tetraisopropoxide plasma. Thin Solid Films. 1 nov 2012;522:366‑71.
45. Vallée C, Goullet A, Granier A. Direct observation of water incorporation in PECVD SiO2 films by UV-Visible ellipsometry. Thin Solid Films. 31 déc 1997;311(1):212‑7.
46. Li D, Dai S, Goullet A, Carette M, Granier A, Landesman JP. Annealing and biasing effects on the structural and optical properties of PECVD-grown TiO2 films from TTIP/O2 plasma. J Mater Sci Mater Electron. 1 août 2018;29(15):13254‑64.
47. Fendler JH, éditeur. Nanoparticles and Nanostructured Films: Preparation, Characterization and Applications [Internet]. 1re éd. Wiley; 1998 [cité 1 mai 2021]. Disponible sur: https://onlinelibrary.wiley.com/doi/book/10.1002/9783527612079
48. Horprathum M, Chindaudom P, Limnonthakul P, Eiamchai P, Nuntawong N, Patthanasettakul V, et al. Dynamic *in situ* spectroscopic ellipsometric study in inhomogeneous TiO2 thin-film growth. J Appl Phys. juill 2010;108(1):013522.
49. Muneshwar T, Cadien K. Probing initial-stages of ALD growth with dynamic in situ spectroscopic ellipsometry. Appl Surf Sci. févr 2015;328:344‑8.
50. Guillard C, Debayle D, Gagnaire A, Jaffrezic H, Herrmann J-M. Physical properties and photocatalytic efficiencies of TiO2 films prepared by PECVD and sol–gel methods. Mater Res Bull. 3 août 2004;39(10):1445‑58.

51. Quesada-Cabrera R, Sotelo-Vázquez C, Quesada-González M, Melián EP, Chadwick N, Parkin IP. On the apparent visible-light and enhanced UV-light photocatalytic activity of nitrogen-doped TiO 2 thin films. J Photochem Photobiol Chem. janv 2017;333:49‑55.